Journal of Magnetic Resonance 388 (2026) 108076

Contents lists available at ScienceDirect

Journal of Magnetic Resonance

journal homepage: www.elsevier.com/locate/jmr

A $^{13}C^{\beta}$ CEST experiment with improved sensitivity for the characterization of protein excited states☆

Jeffrey P. Bonin [a,b,c,*], Lewis E. Kay [a,b,c,*]

[a] Departments of Molecular Genetics and Biochemistry, University of Toronto, Toronto, Ontario M5S 1A8, Canada
[b] Department of Chemistry, University of Toronto, Toronto, Ontario M5S 3H6, Canada
[c] Program in Molecular Medicine, The Hospital for Sick Children Research Institute, Toronto, Ontario M5G 0A4, Canada

ARTICLE INFO

Keywords:
CEST
Excited states
Protein dynamics
Pro-IL-18
Adiabatic decoupling

ABSTRACT

Protein function often relies on transient excursions from highly populated ground states to sparse conformers, or 'excited states'. Unlike most other biophysical methods, NMR spectroscopy provides an avenue for quantifying the kinetics and thermodynamics of such transitions and for obtaining structural insights into the participating conformers through measurement of chemical shifts using experiments such as Chemical Exchange Saturation Transfer (CEST). As in many NMR applications, a trade-off between sensitivity and resolution requires compromises that can negatively impact the quality of the resulting data. One example is the $^{13}C^{\beta}$ CEST experiment which is often recorded using a triple-resonance scheme with readout of backbone amide correlations. The sensitivity hit associated with multiple magnetization transfer steps challenges applications to protein systems with large linewidth contributions from the exchange process that is the focus of the measurements. Here we present a non-constant time $^{13}C^{\beta}$-$^{1}H^{\beta}$ version of the $^{13}C^{\beta}$ CEST experiment that is optimized on a per-residue type basis to provide significant sensitivity improvements over other pulse schemes. The large sensitivity gains in an application to the Q54V variant of pro-interleukin-18 were critical for determination of $^{13}C^{\beta}$ chemical shifts for residues interconverting between the ground state and a pair of excited conformers. Technical details of the experiment are presented.

1. Introduction

Proteins are dynamic molecules whose functions can involve transient excursions from populated and low energy ground states to less populated and higher energy conformations (referred to as excited states in what follows) [1–5]. While efforts in structural biology have largely focussed on characterizing ground state conformers of biomolecules, either via experiment or now by machine learning (ML) approaches [6,7], it has become increasingly appreciated that further studies are required to understand the important roles of dynamics in modulating biomolecular function. Such studies are challenged, however, by the fact that higher energy conformers are transient and sparsely populated so that they can often only be 'observed' indirectly via the ground state. Experiments such as Carr-Purcell-Meiboom-Gill (CPMG) relaxation dispersion [8–11], Chemical Exchange Saturation Transfer (CEST) [12], Dark state Exchange Saturation Transfer (DEST) [13], and $R_{1\rho}$ relaxation dispersion [14–16] provide an avenue for 'seeing the invisible' and have been used to quantify the kinetics and thermodynamics of exchange processes in both proteins [2,17–22] and nucleic acids [23,24], as well as in smaller molecules [25]. Additionally, structural information is available in the form of chemical shifts and residual anisotropic interactions which are sometimes sufficient to generate reliable ensembles of excited state conformers [26–33]. Studies have been performed on a wide variety of different systems, providing insights into mechanisms of enzymatic reactions [2,5], protein folding and misfolding [26,27], ligand binding and molecular recognition [34], and the development of resistance to therapeutic drugs to fight disease [3].

Each of the different NMR methods listed above is ideally suited for studies of dynamics in particular time regimes. In our experience, CEST is particularly attractive for exploring millisecond timescale processes, as the chemical shifts of excited state(s) can be obtained directly from the positions of minor "dips" in CEST profiles, and are not reliant on fitting algorithms locating the global minimum of an error surface, as for the analysis of CPMG data [11]. Further, as CEST experiments probe

☆ This article is part of a Special issue entitled: 'Exchange NMR Spectroscopy' published in Journal of Magnetic Resonance.

* Corresponding author at: Departments of Molecular Genetics and Biochemistry, University of Toronto, Toronto, Ontario M5S 1A8, Canada.
E-mail addresses: jeff.bonin@utoronto.ca (J.P. Bonin), lewis.kay@utoronto.ca (L.E. Kay).

https://doi.org/10.1016/j.jmr.2026.108076
Received 15 March 2026; Received in revised form 22 April 2026; Accepted 22 April 2026
Available online 24 April 2026

invisible states using weak radio-frequency fields, on the order of tens of Hz, they are relatively insensitive to the effects of homonuclear scalar couplings [35], which can create significant artifacts in CPMG experiments. Thus, CEST can be readily applied to studies using backbone and sidechain ^{13}C spins in a uniformly ^{13}C labeled sample [36], enabling a more detailed characterization of the excited state's structure.

Over a decade ago our laboratory proposed a pair of triple resonance-based schemes for recording $^{13}C^{\alpha}$ and $^{13}C^{\beta}$ CEST profiles, with a readout through the amide correlations of the subsequent residue [37]. These experiments have the advantage that the $^{1}H^{N}$-^{15}N spectrum is significantly better resolved than the corresponding $^{1}H^{\alpha}$-$^{13}C^{\alpha}$ or $^{1}H^{\beta}$-$^{13}C^{\beta}$ correlation maps that otherwise would be recorded for these measurements, but the resulting CEST datasets pay a price in sensitivity from the multiple magnetization transfer steps required, particularly for the $^{13}C^{\beta}$-based experiment. While resolution is improved in ^{1}H-^{13}C experiments using constant-time approaches, the sensitivity vs resolution trade-off remains problematic.

Here we describe modifications to the ^{1}H-^{13}C class of CEST experiments for measurement of $^{13}C^{\beta}$ chemical shifts which we developed previously [36], to study conformational dynamics in the 22 kDa protein pro-interleukin-18 (pro-IL-18). The resulting experiment is particularly powerful in cases where only a few $^{13}C^{\beta}$ chemical shifts are required, as for our studies of pro-IL-18, where the region of conformational heterogeneity in the protein had been identified previously [17]. By tailoring experimental parameters to the residue or residue type in question, as has been done previously in ^{13}C-detected experiments focussed on deuterated protein sidechains [38] and in $R_{1\rho}$ experiments on proteins [39] and RNA [40], significant sensitivity enhancements are obtained that enable accurate quantification of chemical shifts of excited states that would not be possible otherwise.

2. Materials and methods

2.1. Sample preparation

Isotopically enriched samples of pro-IL-18 (wildtype, WT, and Q54V) were expressed and purified from *E. coli* using our previously established protocol [41]. Samples comprised 1 mM protein dissolved in 20 mM MES, 50 mM KCl, 0.5 mM EDTA, and 10 mM DTT buffer, pH 6.5, 3% D_2O.

2.2. NMR spectroscopy

NMR experiments were collected at 25 °C for Q54V pro-IL-18 and 40 °C for the WT protein on Bruker AVANCE III HD 18.8 T (800 MHz, $^{13}C^{\beta}$-$^{1}H^{\beta}$ experiments) and AVANCE III HD 14.1 T (600 MHz, triple resonance amide-based experiments) NMR spectrometers equipped with 5-mm TCI triple-axis gradient cryoprobes. Experimental parameters are listed in Table S1; briefly B_1 CEST fields of 27.2 and 27.0 Hz were used for recording $^{13}C^{\beta}$-$^{1}H^{\beta}$ and amide datasets, respectively, with successively sampled frequencies separated by 59.6 (Leu)/48.3 (Ile)/48.7 (Val) and 62.6 (amide data) Hz.

The recorded data were processed with NMRPipe [42], visualized using NMRFAM-SPARKY [43], and peak volumes were fit using peakipy (https://github.com/j-brady/peakipy). Weak B_1 field frequency sampling schedules for CEST experiments were determined using an optimized frequency sampling approach [44]. Adiabatic ^{13}C decoupling, applied during the $^{13}C^{\beta}$ chemical shift encoding as well as the τ_b and τ_c transfer periods, was optimized for each specific amino acid type observed. The wavemaker code for generating the decoupling elements is given in the Supporting Information.

Data analysis.

The $^{13}C^{\beta}$ CEST profile for L56 (AX_2) from the non-CT $^{13}C^{\beta}$-$^{1}H^{\beta}$ experiment was generated by summing the intensities from the L56C^{β}-H^{β}_{A} and L56C^{β}-H^{β}_{B} signals. CEST experiments were analyzed with the ChemEx program (https://github.com/gbouvignies/ChemEx), with $^{13}C^{\beta}$ transverse relaxation rates (R_2) of spins in the ground and excited states constrained to be the same. Populations and exchange rates were fixed to those obtained in on our previous analyses of ^{15}N CPMG and CEST data recorded on WT and Q54V pro-IL-18 [17,45].

3. Results and discussion

3.1. The problem

Using a CPMG/CEST strategy to study conformational dynamics in the 22 kDa protein pro-IL-18, we previously showed that the WT molecule interconverts between a ground state and a pair of excited conformers, ES_1 and ES_2, whose fractional populations are on the order of 0.5% [17]. The low populations of these sparse conformers resulted in small CPMG dispersion profiles ($\sim 5\ s^{-1}$) and in small minor state dips in CEST experiments. A Q54V mutation was shown to stabilize both excited states, increasing their fractional populations by an order of magnitude [45], leading to more pronounced signatures of chemical exchange in both CPMG and CEST datasets. The larger populations were also critical in NOE-based studies to validate structures of ES_1 and ES_2 predicted using the ML program AlphaFlow, a generative model that was, in part, trained on molecular dynamics data [46].

To obtain robust estimates of secondary structure for exchanging regions in both ES_1 and ES_2 we wished to measure $^{13}C^{\beta}$ chemical shifts, supplementing backbone ^{1}H and ^{13}C shifts that were already recorded. However, the increased effective transverse relaxation rates of spins in the Q54V pro-IL-18 variant from elevated exchange contributions, relative to the WT protein, had a deleterious effect on the sensitivity of triple resonance, amide-based CEST experiments that have been typically used in our laboratory to record $^{13}C^{\beta}$ CEST profiles. This results from the large number of magnetization transfer steps from $^{13}C^{\beta}$ to the detected amide backbone spins, as shown in Fig. 1A [37]. A comparison of the resulting 2D CEST $^{1}H^{N}$-^{15}N reference spectra for WT and Q54V pro-IL-18, where the CEST mixing time is set to 0 s, is shown in Fig. 1B **(left)**, along with traces through the peaks indicated by dashed lines, highlighted in Fig. 1B **(right)**. These illustrate the significant sensitivity drop in the spectrum recorded of the mutant. Fig. 1C shows that the poor spectral quality translates into noisy CEST profiles (V55), or even more pathologically, into the complete absence of CEST data (V54).

3.2. A solution

As described above, the sensitivity of our standard triple-resonance-based approach for recording $^{13}C^{\beta}$ CEST was inadequate for studies of the Q54V pro-IL-18 variant. Applications to the WT protein were improved, but still not of high sensitivity, presenting a challenge for quantifying the small dips that derive from the sparse populations of excited states in this case. A second approach would be to record $^{13}C^{\beta}$ CEST spectra as a series of 2D $^{13}C^{\beta}$-$^{1}H^{\beta}$ constant-time (CT) datasets, as we proposed many years ago for uniformly ^{13}C labeled proteins [36]. However, as the dynamic region that we targeted was a small β strand consisting of only five residues, we wondered whether a better strategy might be to record each of the few profiles needed individually, or at least each residue-type separately, with each experiment optimized specifically for the residue or residues in question.

Fig. 2 illustrates the pulse scheme that was developed with this in mind, following very closely the CT-HSQC strategy proposed previously [36]. In the implementation shown in the figure, tailored ^{13}C decoupling using adiabatic waveforms (see Supporting Information) is applied during periods of duration $2\tau_b$ and $2\tau_c$ to suppress evolution resulting from homonuclear scalar couplings involving the $^{13}C^{\beta}$ spin in question and its one bond attached ^{13}C coupling partners. In addition, rather than using a CT-element for recording chemical shift evolution during t_1, which can have a deleterious effect on sensitivity, a non-CT version is implemented with adiabatic ^{13}C decoupling to suppress evolution from homonuclear ^{13}C-^{13}C couplings, as we have done previously in

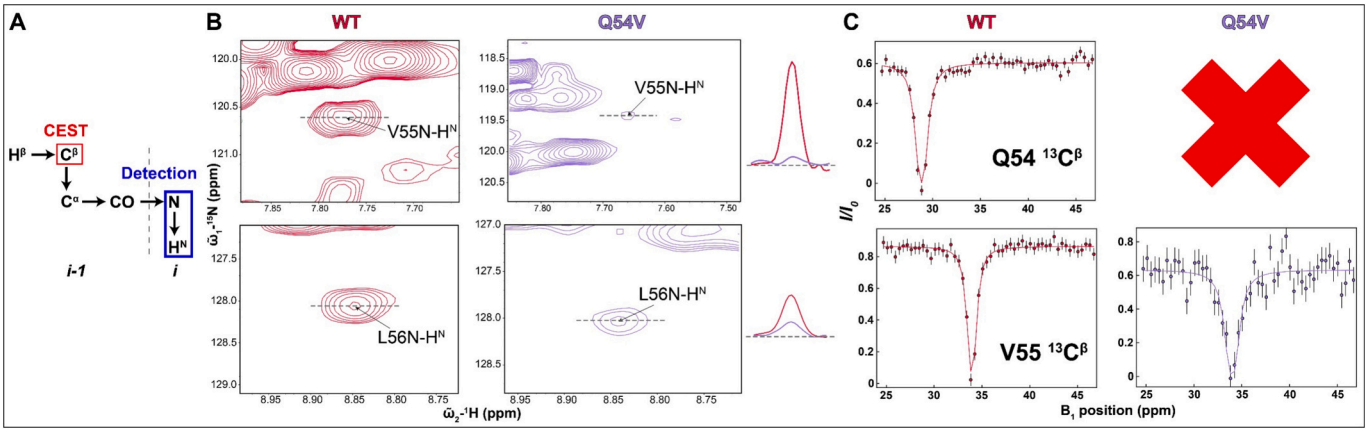

Fig. 1. The triple resonance amide-based $^{13}C^{\beta}$ CEST experiment suffers from poor sensitivity for key exchanging residues in Q54V pro-IL-18. (A) Magnetization transfer pathway for the amide-based $^{13}C^{\beta}$ CEST experiment, starting from the H^{β} of residue *i-1* and recording the amide correlation of residue *i*. In this manner the $^{13}C^{\beta}$ CEST profile of residue 54 is obtained from the intensities of the amide correlation of V55. (B) Selected regions of reference spectra (CEST mixing time set to 0 s) for WT and Q54V pro-IL-18, highlighting amide correlations of V55 and L56, resides that are key probes of conformational exchange in the protein. Traces through the peaks are shown on the right, overlaid for WT (red) and Q54V (purple). Greater exchange broadening of the Q54V pro-IL-18 signals relative to those of the WT protein translates to low intensity amide correlations for the mutant, particularly for V55 whose signal is nearly absent. (C) Q54 and V55 $^{13}C^{\beta}$ CEST profiles, obtained from the intensities of the V55 and L56 amide correlations for WT and Q54V pro-IL-18. The much lower signal-to-noise of the Q54V CEST data prevents accurate determination of $^{13}C^{\beta}$ chemical shifts for the vast majority of residues of the excited states of the protein. (For interpretation of the references to colour in this figure legend, the reader is referred to the web version of this article.)

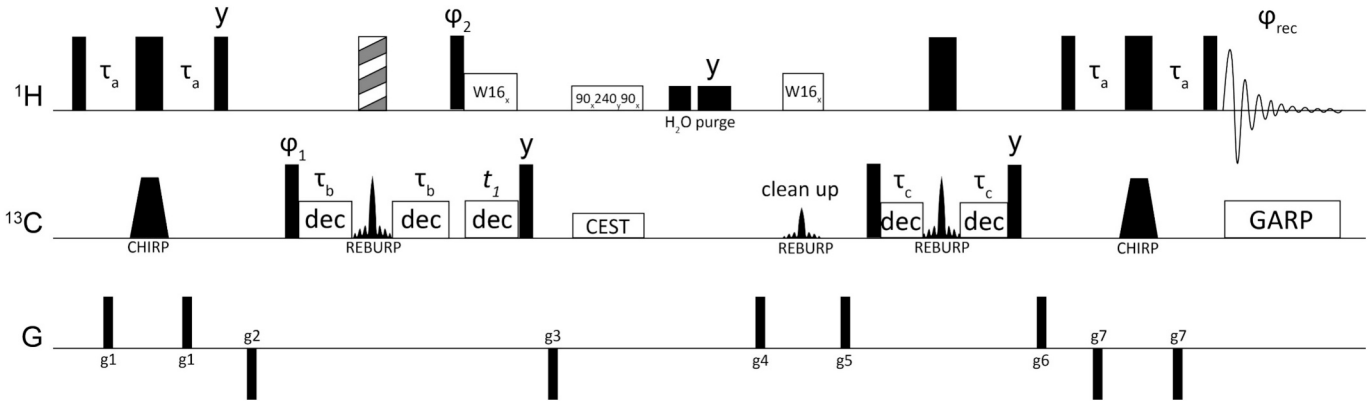

Fig. 2. Sensitivity optimized $^{13}C^{\beta}$ CEST sequence for uniformly ^{13}C labeled proteins with $^{13}C^{\beta}$-$^{1}H^{\beta}$ readout. Narrow (wide) black rectangles denote hard 90° (180°) pulses. 180° shaped pulses are indicated by the non-rectangular shapes, with the type of pulse noted below each shape. The striped rectangular pulse is of the 90y-180x-90y composite variety [47]. Decoupling schemes are indicated by the white rectangles ($W16_x$ = WALTZ16 [48] with pulses along ±x, 6.3 kHz; 90x240y90x = ^{1}H decoupling during CEST [12], ~3.5 kHz; dec = residue or residue-type selective adiabatic decoupling scheme as described in Supporting Information), with the rectangle labeled as "CEST" indicating a weak CEST field (~25 Hz used here). The two rectangles labeled "H_2O purge" are 2 and 3 ms rectangular purge pulses (applied at the same power as the immediately preceding 90x240y90x decoupling element) to dephase water magnetization in applications involving proteins dissolved in H_2O. ^{1}H and ^{13}C carriers were positioned on the water line and at 40.3 ppm (Ile), 45.5 ppm (Leu) and 33 ppm (Val) respectively, except during the CEST period where the ^{1}H carrier was centered on the $^{1}H^{\beta}$ signals of interest and the $^{13}C^{\beta}$ carrier was varied over the appropriate ^{13}C spectral region. CHIRP pulses [49] were 400 μs in duration, ~11 kHz field, and swept ±40 kHz about the carrier; REBURP pulses [50] separating pairs of τ_b and τ_c delays were each 360 μs, 17.5 kHz; the 'clean up' REBURP pulse was 5 ms (1.2 kHz), centered at 40.3 ppm (Ile), 45.5 ppm (Leu) and 33 ppm (Val) and applied in the first four of the eight scan phase cycle. The power levels and durations of REBURP pulses are indicated for applications on an 800 MHz spectrometer; for experiments recorded on an X MHz spectrometer the pulse widths are adjusted according to the relation pw_reburp(X) = pw_reburp(800 MHz) x 800/X. Decoupling during acquisition was achieved with the GARP decoupling sequence [51] using a 2.5 kHz field. Delay durations are: τ_a = 1.8 ms, $\tau_{b,c}$ = 1.85 ms (AX spin system) or 0.925 ms (AX_2). All pulses are applied along the x axis unless otherwise indicated. The phase cycle is: φ_1 = {0,0,2,2}; φ_2 = {1,3}; φ_{rec} = {0,0,2,2,2,2,0,0}. The gradient duration and strengths were as follows: g1 = {300 μs, 6.75 G/cm}; g2 = {1 ms, −18 G/cm}; g3 = {1 ms, −27 G/cm}; g4 = {500 μs, 22.5 G/cm}; g5 = {500 μs, 11.25 G/cm}; g6 = {800 μs, 13.5 G/cm}; g7 = {400 μs, −18 G/cm}. All gradients were applied along the z-axis except for g7, which was applied along the x-axis.

recording $^{13}C^{\alpha}$ CEST profiles using $^{1}H^{\alpha}$-$^{13}C^{\alpha}$ datasets [36]. By means of example, in recording CEST profiles for Val 54 and Val 55, band selective adiabatic fields were applied centered at 61.5 ± 3.5 ppm (C^{α}) and 21 ± 3 ppm ($C^{\gamma 1,2}$). These decoupling elements suppress evolution from scalar couplings, as can be seen in spectral regions of ^{13}C-^{1}H correlation maps focussed on the two valines (compare **Fig. 3A** and **B**), but introduce noise in the decoupled regions (Fig. 3B). The noise can be removed by applying a selective REBURP pulse (labeled 'clean up' in Fig. 2) in alternate scans focussed on the $^{13}C^{\beta}$ resonance positions of the correlations of interest, along with concomitant inversion of the receiver phase, to retain signal originating only from these correlations (Fig. 3C). In this manner the signal-to-noise (S/N) is not compromised by this procedure and although the 'clean up' pulse does introduce an additional two steps to the phase cycle if it is applied as an independent element, it is possible to combine the on/off cycling of the selective pulse with the ϕ_2 phase cycle, reducing the number of steps two-fold. The noise artifacts have an

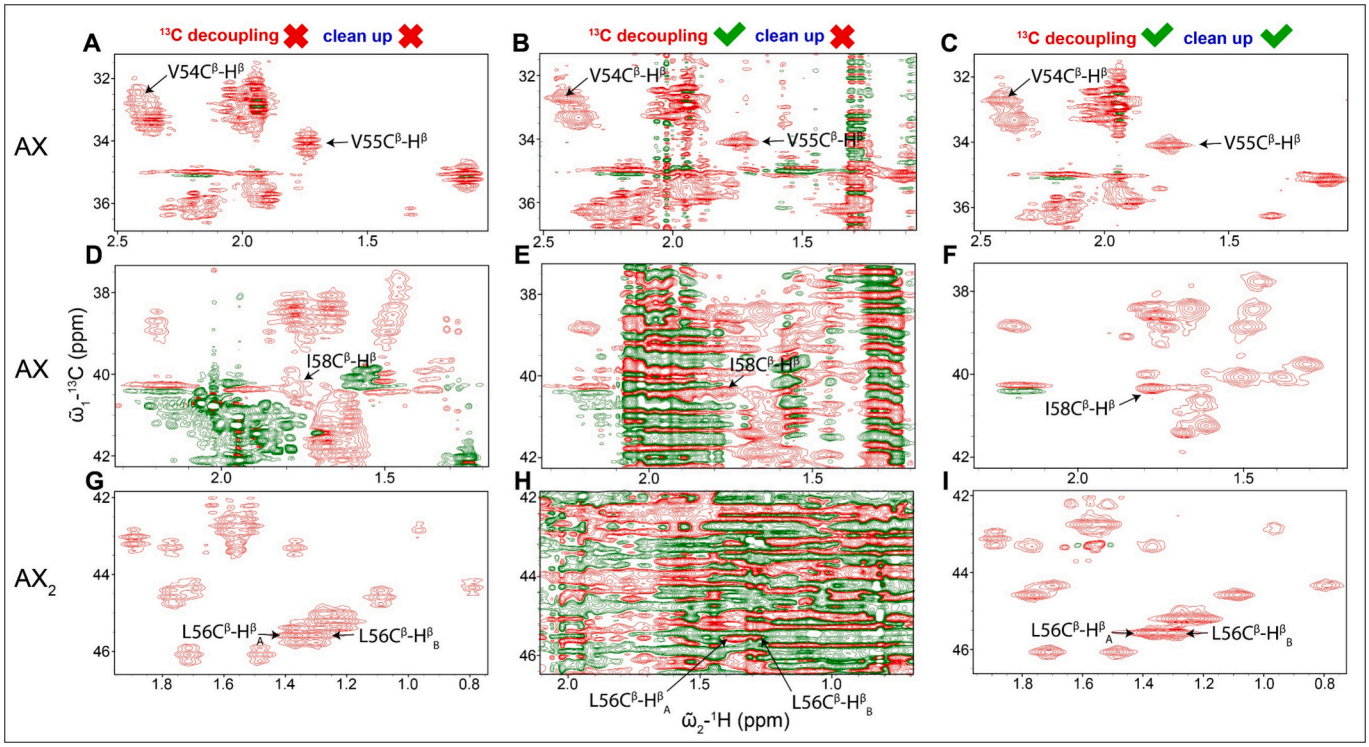

Fig. 3. The adiabatic decoupling scheme suppresses evolution of ^{13}C magnetization from J_{CC} couplings but requires a 'clean up' pulse to remove introduced artifacts. Selected regions from reference CEST spectra (CEST relaxation element set to 0 ms) recorded on Q54V pro-IL-18 highlighting several probes of interest, including V55 and I58 (AX spin system) as well as L56 (AX_2). Spectra were recorded without (A, D, G) and with (B, E, H, C, F, I) adiabatic ^{13}C decoupling during t_1, and with 'clean up' pulses (Fig. 2) applied in (C, F, I). In the absence of ^{13}C decoupling the signals are split into four and three peaks for the AX and AX_2 spin systems, respectively (panels A, D, G). Application of the decoupling element effectively collapses the multiplet components into a single peak but also produces substantial noise arising from ^{13}C$^{\gamma}$ signals which are perturbed by the decoupling (panels B, E, H). The noise can be removed by applying a long, narrow bandwidth REBURP pulse in alternate scans, and concomitant receiver phase cycling, to preserve only the signals of interest and, thus, eliminate the noise (panels C, F, I). Red and green contoured peaks in spectra have opposite phases. (For interpretation of the references to colour in this figure legend, the reader is referred to the web version of this article.)

even more pronounced effect for Ile 58 and Leu 56 (bottom two rows). As the ^{13}C$^{\gamma}$ carbons of Arg, Ile, Leu, and Lys have similar chemical shifts and the corresponding ^{1}H$^{\gamma}$ of these residues resonate in the vicinity of the β-protons of Ile and Leu, the resulting noise completely obscures the ^{1}H$^{\beta}$-^{13}C$^{\beta}$ correlations of interest. However, because the ^{13}C$^{\beta}$ chemical shifts for Leu and Ile are well resolved from the shifts of the 'interfering'

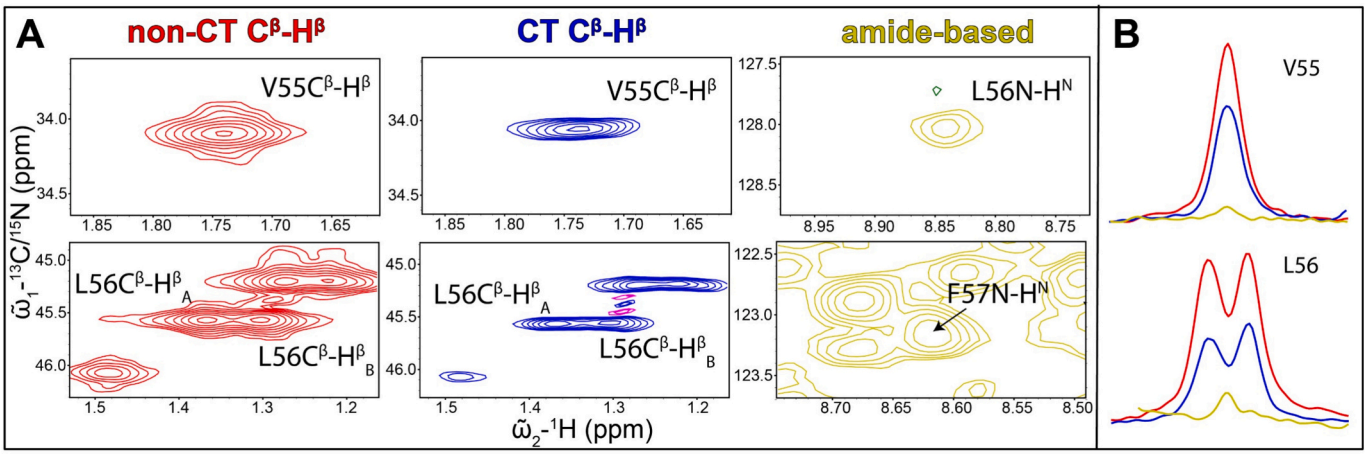

Fig. 4. Non-CT ^{13}C$^{\beta}$-^{1}H$^{\beta}$ experiment yields superior signal-to-noise compared to previous CT ^{13}C$^{\beta}$-^{1}H$^{\beta}$ and amide-based sequences. (A) Selected regions from reference CEST spectra of Q54V pro-IL-18 recorded using the scheme of Fig. 2 (left), previously published CT ^{13}C$^{\beta}$-^{1}H$^{\beta}$ (center), and amide-based (right) sequences, highlighting signals giving rise to ^{13}C$^{\beta}$ CEST profiles for V55 and L56. (B) Traces through the Val 55 and Leu 56 (^{13}C$^{\beta}$-^{1}H$^{\beta}$) or through the Leu 56 and Phe 57 (amide) cross peaks are shown, overlaid for the non-CT ^{13}C$^{\beta}$-^{1}H$^{\beta}$ (red), CT ^{13}C$^{\beta}$-^{1}H$^{\beta}$ (blue), and amide-based (gold) experiments. The traces establish significant sensitivity gains for the ^{13}C$^{\beta}$-^{1}H$^{\beta}$ versions compared to their amide-detected counterpart, and further improvements in signal-to-noise for the non-CT experiment compared to the previous CT version. (Non-)CT spectra were recorded with 8 scans, (145)146 complex points in the indirect dimension, and a 1.5 s interscan delay on an 800 MHz spectrometer. The amide-based spectrum was recorded with 16 scans, 55 complex points in the indirect dimension, and a 2 s interscan delay on a 600 MHz spectrometer. (For interpretation of the references to colour in this figure legend, the reader is referred to the web version of this article.)

$^{13}C^{\gamma}$ carbons, the noise artifacts can, again, be eliminated by using a $^{13}C^{\beta}$ selective 'clean up' pulse, as can be seen in a comparison of Figs. 3E,H and 3F,I. Note that Arg and Met residues are generally incompatible with this approach given that their $^{13}C^{\beta}$ and $^{13}C^{\gamma}$ chemical shifts are nearly degenerate (Arg: $^{13}C^{\beta} = 31 \pm 2$ ppm, $^{13}C^{\gamma} = 27 \pm 3$ ppm, Met: $^{13}C^{\beta} = 33 \pm 3$ ppm, $^{13}C^{\gamma} = 32 \pm 3$ ppm based on BMRB statistics).

Spectra recorded using the non-CT $^{13}C^{\beta}$-$^{1}H^{\beta}$ experiment of Fig. 2 are of higher sensitivity than either of the CT $^{13}C^{\beta}$-$^{1}H^{\beta}$ [36] and triple resonance amide-based [37] versions (Fig. 4). Fig. 4A shows corresponding reference planes for each of the CEST experiments, focussing on correlations from which V55 (top) and L56 (bottom) $^{13}C^{\beta}$ CEST profiles are quantified. Traces through the peaks of interest are shown in Fig. 4B, clearly demonstrating the very substantial increase in signal-to-noise (roughly 10-fold) in the non-CT $^{13}C^{\beta}$-$^{1}H^{\beta}$ experiment compared to the amide detected version. A corresponding increase in signal intensity (1.5 and 2-fold for V55 and L56, respectively) is also obtained relative to the previously published CT-version of the experiment. In the comparison presented, both CT- and non-CT $^{13}C^{\beta}$-$^{1}H^{\beta}$ experiments are recorded with identical numbers of scans and closely matched acquisition times in the indirect (^{13}C) dimensions, while the amide-based dataset was obtained with twice the number of scans. Notably, the signal-to-noise benefits of the non-CT experiment increase as $^{13}C^{\beta}$ transverse relaxation rates get larger. Consequently, the gains in sensitivity with the new scheme will become even more substantial for proteins larger than Q54V pro-IL-18 (193 residues) and/or with more pronounced exchange contributions to linewidths.

As expected, the improved sensitivity of the non-CT $^{13}C^{\beta}$-$^{1}H^{\beta}$ experiment compared to its amide-based counterpart translates into higher quality CEST profiles for studies of dynamics in pro-IL-18 (Fig. 5). In the case of V55, no clear minor dips are observed in the profile from the amide detected experiment (top right), while in the corresponding profile derived from the non-CT $^{13}C^{\beta}$-$^{1}H^{\beta}$ dataset, two minor-state 'humps' are clearly observed on either side of the ground state dip, enabling confident assignments to ES_1 and ES_2 (top left). In the case of L56, the profile from the amide-based experiment contains a single resolved minor dip (bottom right). However, the poor data quality does not enable definitive assignment of this dip to ES_1, ES_2, or to both. In contrast, the high sensitivity of the CEST profile from the non-CT $^{13}C^{\beta}$-$^{1}H^{\beta}$ experiment enables detection of a shoulder that is upfield of the major state dip in addition to a well-resolved minor state dip that can be confidently assigned to ES_2 and ES_1, respectively (bottom left).

A drawback of the current scheme is that profiles must be recorded on a per-residue or per-residue type basis, so that optimal sensitivity can be obtained. The CT $^{13}C^{\beta}$-$^{1}H^{\beta}$ and amide-based experiments, on the other hand, can provide data on all residue types in a single experiment (or a pair of experiments, with each optimized separately for AX/AX_2 $^{13}C^{\beta}$-$^{1}H^{\beta}$ spin systems) in cases where sensitivity is not limiting. Measuring profiles for multiple residue types simultaneously using the scheme of Fig. 2 necessitates larger bandwidths for adiabatic decoupling, leading to artifacts, as we have observed when focussing on the following subset of residues: {Asn, Asp, Leu, Phe, Tyr}. We are currently investigating other, lower power, decoupling schemes that would be more robust in this regard. However, so long as the $^{13}C^{\beta}$ windows for the residues of interest do not overlap there is no penalty in recording time using residue type selective measurements, as is the case for the three residues we considered in Fig. 3 that were critical for validating secondary structures in ES_1 and ES_2. Notably, because the $^{13}C^{\beta}$-$^{1}H^{\beta}$ approach does not involve magnetization transfer through ^{13}CO spins, where relaxation is dominated by chemical shift anisotropy, and hence field dependent, CEST datasets can be recorded at high magnetic fields to partially compensate for the poorer resolution of ^{13}C-^{1}H spectra relative to amide correlation maps (data presented here were recorded at 800 MHz and 600 MHz for the ^{13}C-^{1}H and amide experiments, respectively). In turn, using higher fields has the advantage of increasing the chemical shift difference between spins in ground and excited states, improving the resolution of CEST profiles. In our experience, if a defined region of conformational heterogeneity is established via ^{15}N-based CPMG or CEST experiments, for example, the selective non-CT $^{13}C^{\beta}$-$^{1}H^{\beta}$

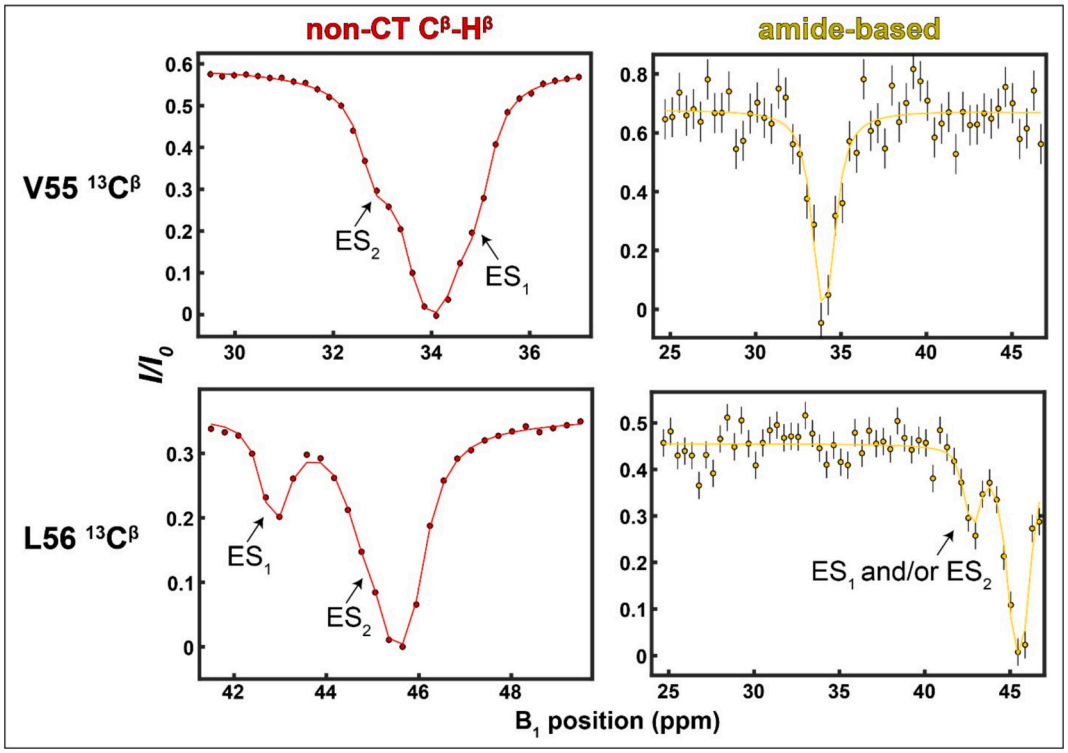

Fig. 5. The non-CT $^{13}C^{\beta}$-$^{1}H^{\beta}$ experiment enables determination of ES_1 and ES_2 $^{13}C^{\beta}$ shifts of Q54V pro-IL-18. $^{13}C^{\beta}$ CEST profiles are shown for V55 and L56 from the non-CT $^{13}C^{\beta}$-$^{1}H^{\beta}$ (left, CEST B_1 field = 27.2 Hz, 800 MHz) and amide-based (right, CEST B_1 field = 27.0 Hz, 600 MHz) experiments, showcasing the dramatic improvement in signal-to-noise associated with the non-CT $^{13}C^{\beta}$-$^{1}H^{\beta}$ version of the experiment.

method provides a facile way to record high quality $^{13}C^{\beta}$ CEST data for key reporter residues of the exchange process.

CRediT authorship contribution statement

Jeffrey P. Bonin: Writing – review & editing, Writing – original draft, Methodology, Formal analysis, Data curation. **Lewis E. Kay:** Writing – review & editing, Writing – original draft, Supervision, Methodology, Funding acquisition, Conceptualization.

Declaration of competing interest

The authors declare the following financial interests/personal relationships which may be considered as potential competing interests: Lewis E. Kay, Jeffrey P. Bonin reports financial support was provided by Canadian Institutes of Health Research. Lewis E. Kay reports financial support was provided by Natural Sciences and Engineering Research Council of Canada. If there are other authors, they declare that they have no known competing financial interests or personal relationships that could have appeared to influence the work reported in this paper.

Acknowledgements

This work was supported through grants from the Canadian Institutes of Health Research (CIHR, FND-503573) and the Natural Sciences and Engineering Council of Canada (024-03872) to L.E.K. J.B. acknowledges salary funding in the form of a post-doctoral fellowship from the CIHR.

Appendix A. Supplementary data

Supplementary data to this article can be found online at https://doi.org/10.1016/j.jmr.2026.108076.

Data availability

Data will be made available on request.

References

[1] M. Karplus, J. Kuriyan, Molecular dynamics and protein function, Proc. Natl. Acad. Sci. 102 (19) (2005) 6679–6685, https://doi.org/10.1073/pnas.0408930102.
[2] S.K. Whittier, A.C. Hengge, J.P. Loria, Conformational motions regulate phosphoryl transfer in related protein tyrosine phosphatases, Science (1979) 341 (6148) (2013) 899–903, https://doi.org/10.1126/science.1241735.
[3] T. Xie, T. Saleh, P. Rossi, C.G. Kalodimos, Conformational states dynamically populated by a kinase determine its function, Science (1979) 370 (6513) (2020), https://doi.org/10.1126/science.abc2754.
[4] J.S. Fraser, M.W. Clarkson, S.C. Degnan, R. Erion, D. Kern, T. Alber, Hidden alternative structures of proline isomerase essential for catalysis, Nature 462 (7273) (2009) 669–673, https://doi.org/10.1038/nature08615.
[5] D.D. Boehr, D. McElheny, H.J. Dyson, P.E. Wright, The dynamic energy landscape of dihydrofolate reductase catalysis, Science (1979) 313 (5793) (2006) 1638–1642, https://doi.org/10.1126/science.1130258.
[6] J. Jumper, R. Evans, A. Pritzel, T. Green, M. Figurnov, O. Ronneberger, et al., Highly accurate protein structure prediction with AlphaFold, Nature 596 (7873) (2021) 583–589, https://doi.org/10.1038/s41586-021-03819-2 (PubMed PMID: 34265844).
[7] Baek M, DiMaio F, Anishchenko I, Dauparas J, Ovchinnikov S, Lee GR, et al. Accurate prediction of protein structures and interactions using a three-track neural network. Science (1979) 2021;373(6557):871–6. doi:https://doi.org/10.1126/science.abj8754.
[8] H.Y. Carr, E.M. Purcell, Effects of diffusion on free precession in nuclear magnetic resonance experiments, Phys. Rev. 94 (3) (1954) 630–638, https://doi.org/10.1103/PhysRev.94.630.
[9] S. Meiboom, D. Gill, Modified spin-Echo method for measuring nuclear relaxation times, Rev. Sci. Instrum. 29 (8) (1958) 688–691, https://doi.org/10.1063/1.1716296.
[10] J.P. Loria, M. Rance, A.G. Palmer, A relaxation-compensated Carr−Purcell−Meiboom−Gill sequence for characterizing chemical exchange by NMR spectroscopy, J. Am. Chem. Soc. 121 (10) (1999) 2331–2332, https://doi.org/10.1021/ja983961a.
[11] D.M. Korzhnev, X. Salvatella, M. Vendruscolo, A.A. Di Nardo, A.R. Davidson, C. M. Dobson, et al., Low-populated folding intermediates of fyn SH3 characterized by relaxation dispersion NMR, Nature 430 (6999) (2004) 586–590, https://doi.org/10.1038/nature02655.
[12] P. Vallurupalli, G. Bouvignies, L.E. Kay, Studying "invisible" excited protein states in slow exchange with a major state conformation, J. Am. Chem. Soc. 134 (19) (2012) 8148–8161, https://doi.org/10.1021/ja3001419.
[13] N.L. Fawzi, J. Ying, D.A. Torchia, G.M. Clore, Probing exchange kinetics and atomic resolution dynamics in high-molecular-weight complexes using dark-state exchange saturation transfer NMR spectroscopy, Nat. Protoc. 7 (8) (2012) 1523–1533, https://doi.org/10.1038/nprot.2012.077.
[14] M. Akke, A.G. Palmer, Monitoring macromolecular motions on microsecond to millisecond time scales by R1ρ−R1 constant relaxation time NMR spectroscopy, J. Am. Chem. Soc. 118 (4) (1996) 911–912, https://doi.org/10.1021/ja953503r.
[15] C. Deverell, R.E. Morgan, J.H. Strange, Studies of chemical exchange by nuclear magnetic relaxation in the rotating frame, Mol. Phys. 18 (4) (1970) 553–559, https://doi.org/10.1080/00268977000100611.
[16] A. Rangadurai, E.S. Szymaski, I.J. Kimsey, H. Shi, H.M. Al-Hashimi, Characterizing micro-to-millisecond chemical exchange in nucleic acids using off-resonance r1ρ relaxation dispersion, Prog. Nucl. Magn. Reson. Spectrosc. 112–113 (2019) 55–102, https://doi.org/10.1016/j.pnmrs.2019.05.002.
[17] J.P. Bonin, J.M. Aramini, L.E. Kay, Structural plasticity as a driver of the maturation of pro-Interleukin-18, J. Am. Chem. Soc. 146 (44) (2024) 30281–30293, https://doi.org/10.1021/jacs.4c09805.
[18] A. Sekhar, J.A. Rumfeldt, H.R. Broom, C.M. Doyle, G. Bouvignies, E.M. Meiering, et al., Thermal fluctuations of immature SOD1 lead to separate folding and misfolding pathways, eLife 4 (2015), https://doi.org/10.7554/eLife.07296.
[19] S. Brüschweiler, P. Schanda, K. Kloiber, B. Brutscher, G. Kontaxis, R. Konrat, et al., Direct observation of the dynamic process underlying allosteric signal transmission, J. Am. Chem. Soc. 131 (8) (2009) 3063–3068, https://doi.org/10.1021/ja809947w.
[20] P.J. Farber, J. Slager, A.K. Mittermaier, Local folding and misfolding in the PBX homeodomain from a three-state analysis of CPMG relaxation dispersion NMR data, J. Phys. Chem. B 116 (34) (2012) 10317–10329, https://doi.org/10.1021/jp306127m.
[21] M. Wolf-Watz, V. Thai, K. Henzler-Wildman, G. Hadjipavlou, E.Z. Eisenmesser, D. Kern, Linkage between dynamics and catalysis in a thermophilic-mesophilic enzyme pair, Nat. Struct. Mol. Biol. 11 (10) (2004) 945–949, https://doi.org/10.1038/nsmb821.
[22] X. Yao, M.K. Rosen, K.H. Gardner, Estimation of the available free energy in a LOV2-jα photoswitch, Nat. Chem. Biol. 4 (8) (2008) 491–497, https://doi.org/10.1038/nchembio.99.
[23] J.T. Baisden, J.A. Boyer, B. Zhao, S.M. Hammond, Q. Zhang, Visualizing a protonated RNA state that modulates microRNA-21 maturation, Nat. Chem. Biol. 17 (1) (2021) 80–88, https://doi.org/10.1038/s41589-020-00667-5.
[24] E.N. Nikolova, E. Kim, A.A. Wise, P.J. O'Brien, I. Andricioaei, H.M. Al-Hashimi, Transient Hoogsteen base pairs in canonical duplex DNA, Nature 470 (7335) (2011) 498–502, https://doi.org/10.1038/nature09775.
[25] V. Ramanujam, C. Charlier, A. Bax, Observation and kinetic characterization of transient schiff base intermediates by CEST NMR spectroscopy, Angew. Chem. Int. Ed. 58 (43) (2019) 15309–15312, https://doi.org/10.1002/anie.201908416.
[26] D.M. Korzhnev, T.L. Religa, W. Banachewicz, A.R. Fersht, L.E. Kay, A transient and low-populated protein-folding intermediate at atomic resolution, Science (1979) 329 (5997) (2010) 1312–1316, https://doi.org/10.1126/science.1191723.
[27] D.M. Korzhnev, R.M. Vernon, T.L. Religa, A.L. Hansen, D. Baker, A.R. Fersht, et al., Nonnative interactions in the FF domain folding pathway from an atomic resolution structure of a sparsely populated intermediate: an NMR relaxation dispersion study, J. Am. Chem. Soc. 133 (28) (2011) 10974–10982, https://doi.org/10.1021/ja203686t (PubMed PMID: 21639149).
[28] P. Neudecker, P. Robustelli, A. Cavalli, P. Walsh, P. Lundström, A. Zarrine-Afsar, et al., Structure of an intermediate state in protein folding and aggregation, Science (1979) 336 (6079) (2012) 362–366, https://doi.org/10.1126/science.1214203.
[29] G. Bouvignies, P. Vallurupalli, D.F. Hansen, B.E. Correia, O. Lange, A. Bah, et al., Solution structure of a minor and transiently formed state of a t4 lysozyme mutant, Nature 477 (7362) (2011) 111–114, https://doi.org/10.1038/nature10349.
[30] P. Vallurupalli, D.F. Hansen, L.E. Kay, Probing structure in invisible protein states with anisotropic NMR chemical shifts, J. Am. Chem. Soc. 130 (9) (2008) 2734–2735, https://doi.org/10.1021/ja710817g (PubMed PMID: 18257570).
[31] J.B. Stiller, R. Otten, D. Häussinger, P.S. Rieder, D.L. Theobald, D. Kern, Structure determination of high-energy states in a dynamic protein ensemble, Nature 603 (7901) (2022) 528–535, https://doi.org/10.1038/s41586-022-04468-9.
[32] K. Madhurima, B. Nandi, S. Munshi, A.N. Naganathan, A. Sekhar, Functional regulation of an intrinsically disordered protein via a conformationally excited state, Sci. Adv. 9 (26) (2023), https://doi.org/10.1126/sciadv.adh4591.
[33] D. De, N. Thapliyal, V. Prakash Tiwari, Y. Toyama, D. Flemming Hansen, L.E. Kay, et al., Mapping the FF domain folding pathway via structures of transiently populated folding intermediates, Proc. Natl. Acad. Sci. 121 (50) (2024), https://doi.org/10.1073/pnas.2416682121.
[34] H. Beach, R. Cole, M.L. Gill, J.P. Loria, Conservation of μs−ms enzyme motions in the apo- and substrate-mimicked state, J. Am. Chem. Soc. 127 (25) (2005) 9167–9176, https://doi.org/10.1021/ja0514949.
[35] Vallurupalli P, Bouvignies G, Kay LE. A computational study of the effects of 13C–13C scalar couplings on 13C CEST NMR spectra: towards studies on a uniformly 13C-labeled protein. ChemBioChem 2013;14(14):1709–13. doi:https://doi.org/10.1002/cbic.201300230.
[36] G. Bouvignies, P. Vallurupalli, L.E. Kay, Visualizing side chains of invisible protein conformers by solution NMR, J. Mol. Biol. 426 (3) (2014) 763–774, https://doi.org/10.1016/j.jmb.2013.10.041.

[37] D. Long, A. Sekhar, L.E. Kay, Triple resonance-based 13Cα and 13Cβ CEST experiments for studies of ms timescale dynamics in proteins, J. Biomol. NMR 60 (4) (2014) 203–208, https://doi.org/10.1007/s10858-014-9868-5.
[38] R.B. Pritchard, D.F. Hansen, Characterising side chains in large proteins by protonless 13C-detected NMR spectroscopy, Nat. Commun. 10 (1) (2019) 1747, https://doi.org/10.1038/s41467-019-09743-4.
[39] D.M. Korzhnev, Vyu Orekhov, L.E. Kay, Off-resonance r1ρ NMR studies of exchange dynamics in proteins with low spin-lock fields: an application to a fyn SH3 domain, J. Am. Chem. Soc. 127 (2) (2005) 713–721, https://doi.org/10.1021/ja0446855.
[40] E.A. Dethoff, K. Petzold, J. Chugh, A. Casiano-Negroni, H.M. Al-Hashimi, Visualizing transient low-populated structures of RNA, Nature 491 (7426) (2012) 724–728, https://doi.org/10.1038/nature11498.
[41] Y. Dong, J.P. Bonin, P. Devant, Z. Liang, A.I.M. Sever, J. Mintseris, et al., Structural transitions enable interleukin-18 maturation and signaling, Immunity 57 (7) (2024) 1533–1548.e10, https://doi.org/10.1016/j.immuni.2024.04.015.
[42] F. Delaglio, S. Grzesiek, GeertenW Vuister, G. Zhu, J. Pfeifer, A. Bax, NMRPipe: a multidimensional spectral processing system based on UNIX pipes, J. Biomol. NMR 6 (3) (1995), https://doi.org/10.1007/BF00197809.
[43] W. Lee, M. Tonelli, J.L. Markley, NMRFAM-SPARKY: enhanced software for biomolecular NMR spectroscopy, Bioinformatics 31 (8) (2015) 1325–1327, https://doi.org/10.1093/bioinformatics/btu830.
[44] N. Bolik-Coulon, D.F. Hansen, L.E. Kay, Optimizing frequency sampling in CEST experiments, J. Biomol. NMR 76 (5–6) (2022) 167–183, https://doi.org/10.1007/s10858-022-00403-2.
[45] J.P. Bonin, J.S. Lee, Z.H. Liu, P.M. Kim, L.E. Kay, Making invisible excited-state structures of pro-interleukin-18 visible by combining NMR and machine learning, Proc. Natl. Acad. Sci. 123 (16) (2026), https://doi.org/10.1073/pnas.2537014123.
[46] B. Jing, B. Berger, T. Jaakkola, AlphaFold meets flow matching for generating protein ensembles, ArXiv (2024), https://doi.org/10.48550/arXiv.2402.04845 arXiv:2402.04845.
[47] M.H. Levitt, R. Freeman, NMR population inversion using a composite pulse, J. Magn. Reson. (1969) 33 (2) (1979) 473–476, https://doi.org/10.1016/0022-2364(79)90265-8.
[48] A.J. Shaka, J. Keeler, T. Frenkiel, R. Freeman, An improved sequence for broadband decoupling: WALTZ-16, Journal of Magnetic Resonance (1969). 52 (2) (1983) 335–338, https://doi.org/10.1016/0022-2364(83)90207-X.
[49] R. Fu, G. Bodenhausen, Broadband decoupling in NMR with frequency-modulated 'chirp' pulses, Chem. Phys. Lett. 245 (4–5) (1995) 415–420, https://doi.org/10.1016/0009-2614(95)01037-A.
[50] H. Geen, R. Freeman, Band-selective radiofrequency pulses, J. Magn. Reson. (1969) 93 (1) (1991) 93–141, https://doi.org/10.1016/0022-2364(91)90034-Q.
[51] A.J. Shaka, P.B. Barker, R. Freeman, Computer-optimized decoupling scheme for wideband applications and low-level operation, J. Magn. Reson. 64 (3) (1969) 547–552, https://doi.org/10.1016/0022-2364(85)90122-2.